IOP PUBLISHING JOURNAL OF PHYSICS D: APPLIED PHYSICS

J. Phys. D: Appl. Phys. **40** (2007) 3592–3607 doi:10.1088/0022-3727/40/12/008

Plasma dynamics in the PF-1000 device under full-scale energy storage: II. Fast electron and ion characteristics versus neutron emission parameters and gun optimization perspectives

V A Gribkov[1,2,3,5], A Banaszak[4], B Bienkowska[2], A V Dubrovsky[1], I Ivanova-Stanik[2], L Jakubowski[4], L Karpinski[2], R A Miklaszewski[2], M Paduch[2], M J Sadowski[4], M Scholz[2], A Szydlowski[4] and K Tomaszewski[2]

[1] A I Alikhanov Institute for Theoretical and Experimental Physics, Bolshaya Cheremushkinskaya ul. 25, Moscow 117218, Russia
[2] Institute of Plasma Physics and Laser Microfusion, ul Hery 23, Warsaw 01-497, Poland
[3] Abdus Salam International Centre for Theoretical Physics, Strada Costiera 11, Trieste 34014, Italy
[4] Andrzej Soltan Institute of Nuclear Studies, Otwock-Swierk 05-400, Poland

E-mail: gribkovv@yahoo.com

Received 28 June 2006, in final form 22 February 2007
Published 4 June 2007
Online at stacks.iop.org/JPhysD/40/3592

Abstract
Electron and ion beam dynamics of the PF-1000 facility were investigated for the first time at its upper energy limit (≈1 MJ) in relation to neutron emission, the pinch's plasma ('target') characteristics and some other parameters with the help of a number of diagnostics with ns temporal resolution. Special attention was paid to the temporal and the spatial cross correlations of different phenomena. Results of these experiments are in favour of a neutron emission model based on ion beam–plasma interaction with three important features: (1) *the plasma target is hot* and confined during a few *'inertial confinement times'*; (2) the *ions* of the main part of the beam are *magnetized* and *entrapped* around the pinch plasma target for a period *longer than the characteristic time of the plasma inductive storage system* and (3) *ion–ion collisions* (both *fusion collisions*, due to head-on impacts and *Coulomb collisions*) are *responsible for neutron emission.* Analysis has shown that one of the ways for achieving a future improvement in the neutron yield of the PF-1000 facility may by changing the geometry of the device. It may ensure an increase in both the discharge current and the initial working gas pressure, eventually resulting in the neutron yield boost.

1. Introduction

Dense plasma focus (DPF) [1,2] is a gas-discharge installation of *Z*-pinch class. It has two coaxial electrodes with the internal one spanned by an insulator. After applying a voltage between the electrodes and breakdown of a filling gas along the insulator's surface such a discharge undergoes two general phases [1–4].

(1) A relatively long magneto-hydrodynamic (MHD) stage (several microseconds), during which a plasma-current sheath (PCS) is accelerated to the chamber axis and imploded

[5] Author to whom any correspondence should be addressed.

on it thus forming a 'pinch'; after this implosion (so-called 'first compression') the plasma column is confined for a time interval Δt equal to several (n) inertial periods of time $\Delta t = n\tau = nr/v_i = nr/(3kT/m_D)^{1/2}$ (where r is the pinch radius, v_i is the thermal ion velocity, k is the Boltzmann constant, T is the plasma temperature and m_D is the deuteron ion mass) and eventually it is disturbed by MHD instabilities (mainly by the Rayleigh–Taylor one) having an increment of about $10^8\,s^{-1}$.

(2) A short kinetic (K) stage (with an assortment of characteristic times of microinstabilities ranging in the interval 10^{-13}–10^{-10} s) when the pinch, already MHD-perturbed, is destroyed by micro- and macroinstabilities during the above period Δt.

As was measured by many researchers right from the start of the DPF phenomenon investigations (50 years ago, see references in [1,2]) a consequence of the perturbation of a plasma column (pinch) is the generation of powerful beams of fast electrons (e) and ions (i) having particle energy in the range extending to hundreds of keV and a few MeV (for electrons and deuterons, respectively). After generation of these e- and i-beams, intense emissions of hard x-rays (HXRs) and fusion neutrons (N) are produced. The latter type of radiation takes place in the operation of a DPF with deuterium (DD) as in the case of PF-1000 or with a deuterium–tritium (DT) mixture used for the filling of its chamber as a working gas under the initial pressure of a few Torr.

Energy E_c, stored in capacitors for a subsequent release to the discharge, occupies a range from just a few Joules [3,4] to about 1 megaJoule (MJ) [2]. The main interest in the installation of its highest energy level operation is connected with a favourable scaling law for the neutron production yield—$Y_n \sim E_c^2$ or $Y_n \cong 10^{10} I_p^4$ (sometimes $Y_n \sim I^5$ [1,2], in particular for the same device [4]). The scaling type is valid for deuterium as a working gas, where I is a discharge current and I_p is the part of the total current which *flows through the dense plasma pinch*, measured in MA. The operation of a DPF with the deuterium–tritium mixture produces an increase in the neutron yield by a factor of about 100 [5]. This means that on the level of a 10 MA current a DPF might produce the same neutron yield as modern pulsed fission reactors, differing from them however by a much shorter neutron pulse duration—a few hundreds of ns—and by an almost monochromatic spectrum centred near 14 MeV. This would open opportunities for many applications in science (e.g. in neutron spectrometry due to the very high 'quality' of the source, $q \geqslant 10^{37}$ [neutrons s^{-3}]) and technology (e.g. in radiation material sciences—see paper I [6]).

As was shown in many publications (see first of all [7] and also the references in [1,2]) the major mechanism responsible for neutron emission in DPF is the interaction of deuterons of 'medium' energy (50–150 keV) with a 'target' (pinch), which is a hot ($\leqslant$ 1 keV) and relatively dense ($\leqslant 10^{19}\,cm^{-3}$) plasma (the so-called 'gyrating particle model'—(GRM)). Here we use the term 'medium energy' for the ion energy of a magnitude well above the thermal one for ions of the pinched plasma ($\sim$1 keV) but much lower than the upper limit of the accelerated deuterons registered ($\sim$ a few MeV). The Larmor radius of these medium-energy deuterons in the magnetic field of the pinch is much smaller compared with the size of the pinch itself thus providing an opportunity to entrap them for a period longer than a simple direct fly-out time.

Paper I presented our recent results taken during the investigation of the PF-1000 facility on an energy level close to the maximal one ($\sim$0.85 MJ). In that paper we paid special attention to different scenarios of the dynamics of the *pinch's plasma* (*target*) depending on various modes of the device operation. Here we shall concentrate our attention on the *generation of charged particle beams* and *their interaction* with the above-mentioned plasma and with the anode. The concept of the fast particle generation mechanism in DPF was developed in [3, 4]. It is based on electron magneto-hydrodynamics (EMH) theory [8] and uses the model of a 'virtual plasma diode', which appears due to anomalous resistivity, springing up in the pinch and constituting the current abruption phenomenon. Within this diode, first fast electrons are accelerated towards the anode and then they are magnetized and substituted by fast ions. The magnitudes of both beam currents are of the order of the total discharge current. The ion beam is aimed in the direction opposite to the electron stream—towards the cathode. Processes of interaction of both e- and i-beams with targets also have a non-trivial character, and they were the subject matter of the above-cited works. In this paper we examine the e- and i-*beams dynamics on the upper level of the DPF energy* in relation to the target evolution (paper I) and the neutron emission in view of the above-mentioned models. So the issue is whether the same physics is true at an energy level of the device an order of magnitude higher than those previously exploited.

2. The apparatus

The PF-1000 device [9] is a DPF of the Mather type [1, 2] operating with deuterium as a working gas at an energy level up to 1 MJ. It was designed about 30 years ago and manufactured on the basis of the technology used in those days. However, this is the only kind of facility being used at the present time with which one can investigate mechanisms of neutron generation within a DPF on an MJ energy level.

Yet its neutron yield at the present time is quite far from those deduced from the above-mentioned law of neutron yield dependence on *energy* stored in the bank (it should be on the level of 10^{13} neutrons per shot whereas the yield is actually equal to 6×10^{11} for the best shot and 2×10^{11} for the typical 'good' ones as seen in this paper). The PF-1000 construction (described in [9] and in paper I [6]) consists of the following main units (positioned on three different floors of the IPPLM building).

- Condenser bank, coaxial cables and a collector of diameter 3 m (figure 1(*a*) and the left-hand side of figure 1(*b*)), charger and pulsed electrical circuit with high-pressure spark-gaps.
- Vacuum chamber (figure 1(*b*) with coaxial electrodes of Mather-type geometry [1, 2] (see also figure 2 of paper I [6]) and vacuum/gas handling systems.

The cylindrical copper anode ($\varnothing = 230$ mm, $l = 600$ mm) is closed by a lid, having the same or a slightly larger diameter as the tube, i.e. a circular hat-shaped 'cap' at its end. If the anode has this cap of a larger diameter, it would be an obstacle

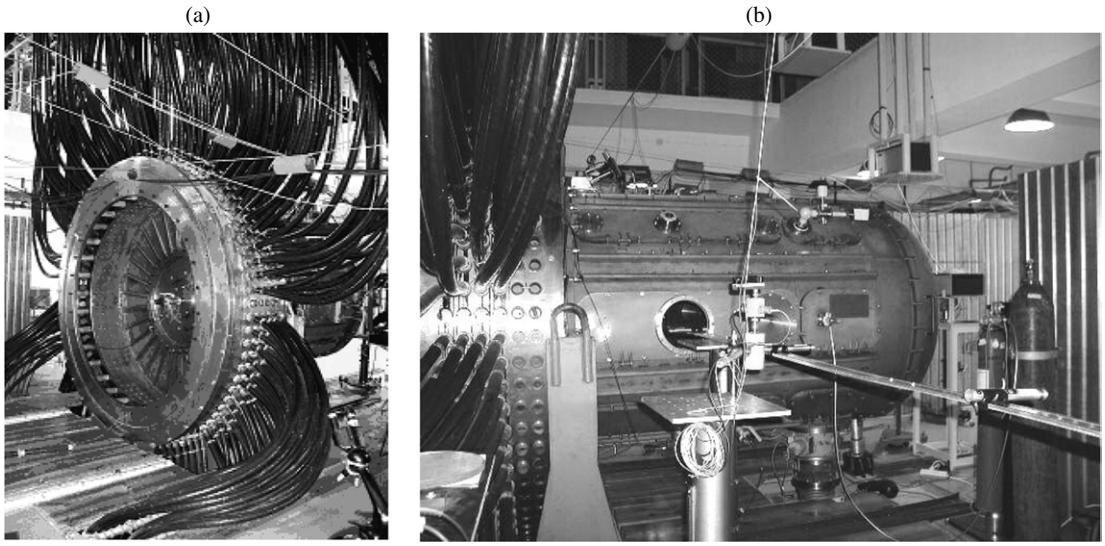

Figure 1. PF-1000: current collector with cables (*a*) and vacuum chamber with the collector (*b*).

for a PCS, which will bifurcate into two parts (see paper I [6]). Two modifications of the cathode electrode geometry of squirrel cage type differing essentially by their inter-electrode gaps, as well as by the lengths and the shape of the rods, were used in this set of experiments. The cathode stainless steel bars were much longer than the anode in the first case whereas both electrodes were equal in length in the second configuration. Their modes of operation, resulting mainly in differing MHD *plasma dynamics*, are also discussed in paper I.

An alumina insulator envelops the anode at its lower part. Its main part extends 113 mm along the anode into the vacuum chamber. The condenser bank of total capacitance 1320 μF (264 capacitors of 5 μF capacitance and 40 nH inductance each) is charged in these experiments to voltage U_0 ranging between 27 and 36 kV. It corresponds to discharge energies E_c within the limits from 480 kJ to 850 kJ. Usually its energy and voltage are equal to 810 kJ and 35 kV, respectively. The energy increase in this set of experiments with PF-1000 compared with the previous ones (see, e.g., [10]) was made by the *bank capacitance increase* (not by the voltage change as in other previous experiments made in Frascati, Stuttgart and Düsseldorf). And as usual the electrode sizes were increased in comparison with previous experiments to match the external and internal inductances of the gun and to equalize the current quarter of the period with the plasma collapse time at this energy magnitude. Typical oscilloscope traces of current and voltage taken at the charging voltage of battery equal to 27 kV are presented in figures 2 (*a*) and (*b*), respectively. They look similar in all the cases of electrode geometries.

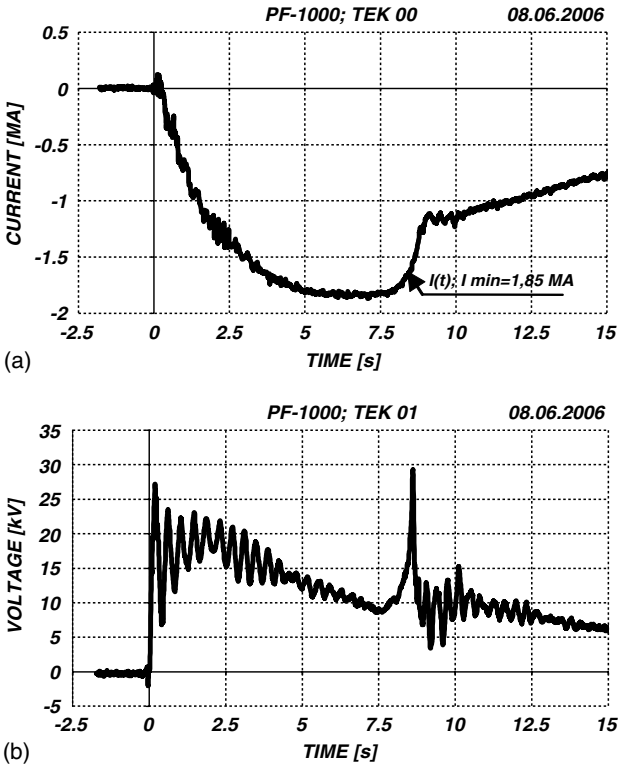

Figure 2. Current (*a*) and voltage (*b*) waveforms of the PF-1000 taken at $U_0 = 27$ kV.

3. Experimental arrangement

To study the MHD evolution of plasma a *streak* camera with a slit parallel to the anode surface and a three/four *frame optical* camera with an exposure time of about 1 ns were employed (see their description in paper I [6]). Two types of three/four *frame soft x-ray* (SXR) cameras—one based on an open microchannel plate (MCP) device in conjunction with a pinhole camera and another just a time-integrated pinhole camera with an x-ray film registration—have been applied in order to obtain plasma images in the SXR range (see details in paper I [6]).

Fast electron beams generated in the DPF were investigated registering HXR radiation produced by them on the anode. This was done with the help of photomultiplier (PM) tubes plus scintillators (PM+S). These beams were also registered directly by means of Cerenkov-type detectors (figure 3) positioned down-stream *in relation to the principal e-beam direction of propagation* (i.e. at the backside of the anode).

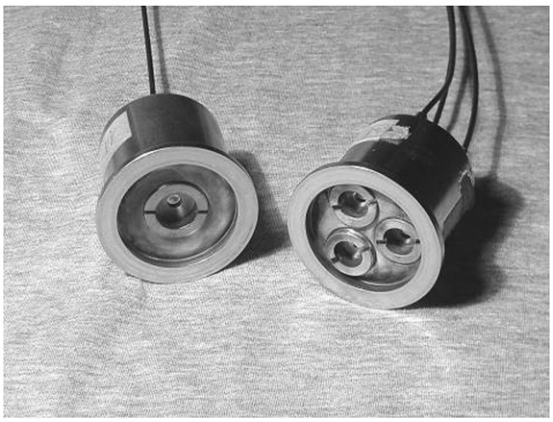

Figure 3. Cerenkov detectors.

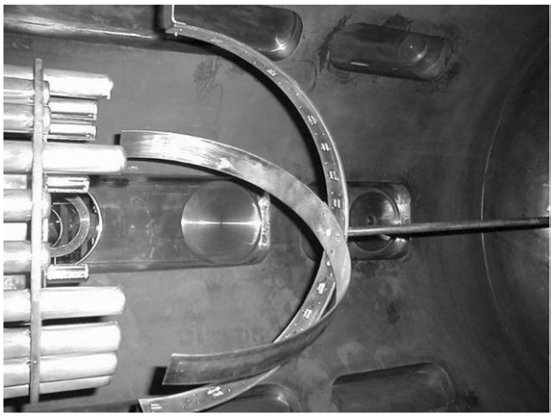

Figure 4. Scheme of track detectors mounting.

These detectors were composed of rutile crystals covered with Cu foils of different thicknesses, and they were coupled with fast PMs through optical cables. The energy of fast electrons which can be registered by this method depends on the crystals used and the filters placed in front of them: without foils, >35 keV; with foils, either above 80 keV or above 120 keV. Signals from them were observed with a fast oscilloscope in correlation with signals from other diagnostic tools.

In order to define the emission characteristics of fast ions (deuterons) in relation to the neutron production process (i.e. ion fluxes, ion angular distributions, ion source location etc) direct ion measurements of fast deuteron beams were performed within the PF-1000 device. An angular distribution of fast deuterons has been measured with nuclear track detectors (of the PM-355 type), placed at a distance of 550 mm from the inner electrode. The semi-ring, where a number of ion track detectors is located, can be seen in figure 4. Each of these detector samples was covered with different Al-foil filters. Ions have been registered at various angles to the electrode axis. To investigate the spatial distribution of fast ions and their trajectories beyond the pinch, miniature ion pinhole cameras have been used. They were positioned at a number of angles to the anode's axis. These cameras were also equipped with the same nuclear track detectors. In order to estimate the energy of the observed deuterons, the detector samples were shielded with Al-foils of different thicknesses. Some temporal and spatial characteristics of the ion beam and its dynamics were obtained by means of an optical multi-frame camera.

Time-resolved SXR signals were measured by means of PIN diodes covered with different filters and by PM tubes also shielded by different foils. Signals from these two types of SXR measuring techniques were compared with other oscilloscope traces (voltage waveforms, dI/dt signals, Cerenkov-detector signals and neutron/HXR pulses) in order to determine their cross correlation. The SXR signal detected by the PIN diodes was also used for synchronization purposes and for the determination of the temporal relation between the maximum of SXR radiation of the plasma and the frame images recorded by means of optical and x-ray diagnostics. Special electrical and optical synchronization arrangements allowed synchronization of the optical diagnostics and other DPF time-resolved diagnostics with a precision of 5 ns.

We investigated the neutron production process by measuring its time evolution, absolute neutron yield and its

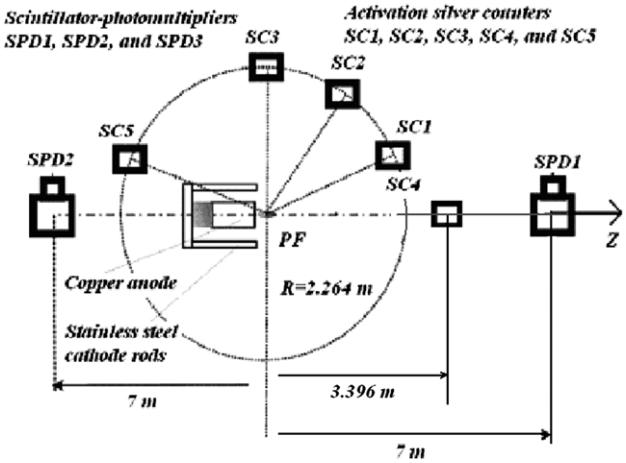

Figure 5. Electrode set-up also showing the positions of the neutron activation counters (SCs) and the fast probe (PM+ scintillator) detectors (SPD) in relation to the Z-axis of the facility.

anisotropy on the basis of both time-integrated methods and time-resolved registration of neutron pulses at different angles to the electrode axis as well as by their comparison with time-resolved and time-integrated measurements of SXR and HXR radiation and the fast electron and ion beams. The total neutron yield (Y_{tot}), i.e. the number of neutrons produced during a single discharge ('shot') and emitted in various directions, was measured taking into consideration the data received by means of five silver-activation counters (SCs) placed at equal distances (3.396 m) in the head-on direction for ion propagation, i.e. in the direction of the Z-axis (SC4), as well as at different angles to it (30°, 60°, 90° and 150° for SC1, SC2, SC3 and SC5, respectively) around the PF-1000 experimental chamber (figure 5).

Independently these measurements were verified by the use of indium-activated counters and so-called 'bubble detectors'. Calibration of *all* detector types was made simultaneously by placing the AmBe isotope neutron source inside the DPF chamber at the position of the plasma pinch. Three scintillator–PM detectors (SPD), located at different angles (all of them at a 7 m distance from the electrode outlet), were used to perform time-resolved measurements of the HXR radiation and N emission with their pulses being separated on the oscilloscope traces due to the corresponding time-of-flight (TOF).

4. Experimental results

Our main series of observations at the PF-1000 facility devoted to the beam generation investigation were carried out in the operational regime with the deuterium pressure ≅2–4 Torr and with a discharge energy of 810 kJ. In these series the chamber had long cathode rods. The anode's cylinder was smooth and even with its flush-mounted head (i.e. *without* a protrusion).

The obtained results, in relation to the discharge current, can be summarized as follows.

(1) The amplitude of the *total* discharge current measured by the Rogowski coil, positioned in close vicinity to the cathode rods inside the DPF chamber, in typical discharges was 2.5–2.6 MA, being sometimes close to 3 MA for the best DPF shots. However, it is much less than the expected one for such an energy of the bank according to the following *experimental* scaling law valid for DPF devices within the above-mentioned energy range (increasing a bank, one has to pay attention that an inductance magnitude is decreased not simply linearly with the number of capacitors but as a root-square dependence on them because of the cables' length and the adding of pre-collectors [3,4]):

$$I_{\text{tot}} \cong U_0 \times (N)^{1/2} \times (C/L)^{1/2} \cong 3.3 \times 10^4 \times 16.3 \times (C[\text{F}]/L[\text{H}])^{1/2} \cong 6.0\,\text{MA}, \quad (1)$$

where $U_0 = 33$ kV is the initial charging voltage of the bank, $N = 264$ is the number of capacitors constituting the bank and $C = 5\,\mu$F and $L = 40$ nH are the capacitance and the inductance of a single capacitor of the bank. Unfortunately attempts to increase this magnitude by a maximization game with the initial pressure and the charging voltage of the device were not crowned with success.

(2) No attempts to measure the *pinch* current I_{p} were made during these experiments, i.e. there are no experimental data on the part of the total current flow actually through the dense plasma column (see paper I [6]). However, substitution of the *total measured current value* into the neutron scaling law gives the following figure expected of the PF-1000 operation:

$$Y_{\text{n}} = 10^{10} \times I_{\text{tot}}^4 = 10^{10} \times (3[\text{MA}])^4 = 8.1 \times 10^{11}, \quad (2)$$

that is, only 35% more than the best experimental magnitude and 4 times more than the mean one. The latter result signifies that the estimated *average pinch current* was about 1.4 times less compared with the total one. This is a reasonable value: $I_{\text{p}} \cong 2$ MA, which is consistent with the data known from the literature [1,2] and deduced from the other results in paper I [6].

(3) Plasma dynamics was investigated in paper I [6]. Here we present four frame-by-frame pictures taken in the visible range in one shot (figure 6). They demonstrate plasma pinch formation ('first compression'—(1), (2)), filament creation (3), i.e. a process of free-streaming of runaway electrons along the Z-axis in its opposite direction, and the start of MHD perturbation of the boundary of a pinch (4). The exposure time is 1 ns and time intervals between the frames is ∼10–20 ns.

(4) A diagram of the angular distribution of neutron emission is presented in figure 7. It was measured by the above-mentioned 5 SCs for shot No 3121 produced at an initial pressure of 465 Pa and a charging voltage of 35 kV (thus, the total energy in the bank was about 0.810 MJ). One can see that under these conditions the anisotropy of the emission measured in the laboratory coordinate frame has a so-called 'normal' character (i.e. it is characterized by a preferential direction of neutron irradiation at 0° to the Z-axis) and its magnitudes are equal to about 1.8 for the ratio Y_{0°/Y_{90° and to ≅0.65 for the ratio $Y_{180^\circ}/Y_{90^\circ}$.

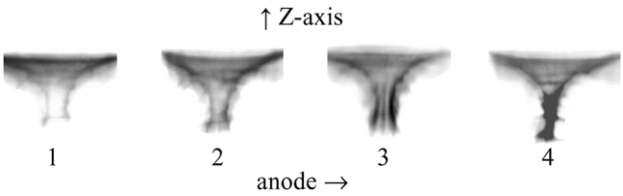

Figure 6. The time sequence of plasma compression stages.

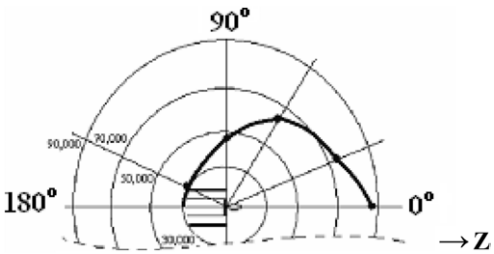

Figure 7. Angular distribution of the PF-1000 neutron yield.

(5) Under these conditions the total neutron emission yield calculated by integrating the data over all 5 silver counters was of the order of 5×10^{10}–2×10^{11} neutron/shot with the maximum neutron yield of 6×10^{11} neutron/shot measured by silver and supported by indium activation counters. Bubble detectors (positioned only at the angle of 90° in these experiments) gave us, in these discharges, a 30% smaller value.

(6) Two neutron pulses were observed in most cases. The second pulse was higher in amplitude by four–ten times compared with the first one (figure 8). The duration of each pulse (FWHM) as well as the interval between them at their registration in the 'head-on' direction were about 150 ns (except for the case of a 'cusp geometry'—see paper I). Compared with smaller devices the first pulse is relatively much larger (usually it was 1–5% of the second one in small DPF whereas here it is 10–25%) and they both have greater longevity (thus in the range of the DPF bank energy from 0.1 to 800.0 kJ the neutron pulse duration increases from 4–5 ns to 150 ns, i.e. it is roughly proportional to the current value).

However, one can see the difference in the neutron pulse shapes (and their duration) for two dissimilar directions of investigation. Namely, at 90°-observation ('side-on') both pulses are longer and look smoother compared with the 'head-on' measurements (0°).

It should be mentioned here that the data in figures 7 and 8 have a rather crude character. Indeed the environment, walls, columns, ceiling and floor, made up of concrete, elements of the DPF construction and capacitors of the main bank in particular, are positioned at distances of 1.5 through 10 m from the chamber or from the counters. It means that the TOF of *primary scattered streams* of 2.45 MeV neutrons along the

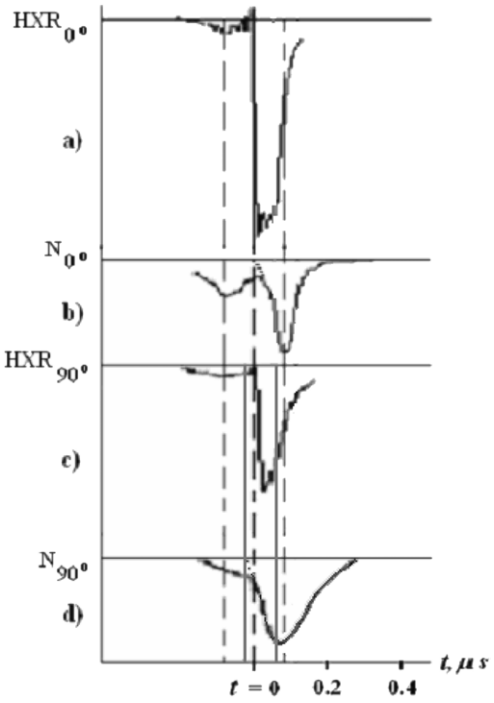

Figure 8. HXR pulses (*a*) and (*c*) versus neutron pulses (*b*) and (*d*) taken at 0° and 90° to the *Z*-axis after moving them forward according to their real (HXR) and assumed (N) TOF.

paths from these elements to the counters (1.5–30 m) is about 75–1000 ns which makes the absolute measurements position-dependent and problematic. Moreover our analysis has shown inequality of the two directions. Namely, the PM tube situated in the *Z*-direction has almost nothing in the hall for single-reflected neutrons to it (a hatch beneath the chamber and a door and a window behind the detector are wide) whereas the side-on PM tube has a wall and columns just near it. These 'obstacles' scatter neutrons and thus give additional primary streams onto the scintillators. Taking into consideration the particular TOF of scattered neutrons it should be admitted that the real shapes of the neutron pulses are distorted especially after their maxima (i.e. in their 'tails'). However, it is evident that such an environment cannot influence the position of the N-pulse *summit* in both cases. This is why the rise-time of pulses in both directions is similar (see figure 8), whereas the pulse decay time is much longer at the side-on observation.

At the same time our activation counters summarize the total yield over a long period (1 min) (figure 7). So they are irradiated by *repeatedly scattered* neutron streams (low-intensity but long-lasting radiation). This is why the data on the neutron yield anisotropy seem to be exaggerated in the normal direction to the *Z*-axis.

In any case these results gave us important and qualitatively correct as well as quantitative information. In the future they need to be verified by a computer simulation of the neutron field evolution in this particular environment, which would give a possibility of better interpretation of the numerical results obtained in such an experiment.

(7) As we mentioned in paper I it was found that for each value (p_0) of an initial filling pressure there is an optimal charging voltage (U_0), which ensures the maximal neutron yield (Y_n). Thus, the initial pressure increase produced *in parallel* to the charging voltage rise during the operation of the facility (provided that for *each initial pressure* we used the above *optimal* initial charging voltage) resulted in a further increase of the neutron yield. *No saturation in the neutron yield was found by this strategy till* 4 Torr *and* 35 kV.

(8) HXR and neutron signals presented in figure 8 are essentially the same as those given in figure 9 of paper I. But in this case we have moved forward both HXR pulses of each oscilloscope trace ((*a*), 0° and (*c*), 90°) by their TOF to a 7 m distance (23.3 ns). At the same time for both neutron emission pulses we have adopted the same procedure for *their* TOF ((*b*), 0° and (*d*), 90°) *as if these neutron pulses consist exactly of* 2.45 MeV neutrons, namely, by 323 ns. It is clearly seen that the *first pulses* of both HXR and N emissions almost *coincide in both cases* (0° and 90°) after their correction by TOF. This means that in the PF-1000 device runaway electrons are accelerated during or slightly earlier in comparison with a so-called first compression phase as in other devices [3,4], and neutron emission produced during this period of time (i.e. in the first pulse) has an energy spectrum centred at 2.45 MeV.

In contrast, second N pulses in the two directions start and have their peaks at later moments compared with the second HXR pulses. Namely, they have their maximal value during a decay time (droop) of the HXR pulses. Moreover the second pulse maximum *in the head-on case* comes earlier than those in the *side-on case* and 'runs over' the HXR pulse. It means (and we might expect it from our anisotropy measurement and the literature) that the spectrum of neutrons irradiated at 0° has higher energy than the neutrons propagating at 90°. Comparing these data with figure 7 one can really see that with the angle variation higher neutron yield corresponds to higher energy of neutrons. It supports results usually being received in smaller devices. We shall discuss it in more detail later in correlation with other diagnostics data.

Two special features of these oscilloscope traces in correlation with frame pictures and with fast particle and neutron generation mechanisms are the following.

(a) The start moment of the second pulse of the HXRs ($t = 0$) being very sharp (in fact it is out of the temporal resolution of our diagnostics) precisely coincides with the appearance of the disruption at the plasma column as was described above. It is seen in figure 6 (4) and is shown in figure 9 by a '↔'-mark. The sequence of pictures shows the column break with the plasma streaming along the circumference and having a meniscus shape (see discussion of this phenomenon later in this paper). Pictures are taken for the anode with an obstacle and short cathode rods—see paper I [6].

(b) The second neutron pulse starting at the same time or a bit later compared with the second HXR pulse reaches its peak when the HXR pulse is over already.

(9) The group of traces (figure 10) taken in a single shot with the whole set of diagnostics presents examples of typical waveforms displaying from top to bottom (a) HXRs from PMT (8–30 keV), (b) SXRs from PMT (3–8 keV), (c) SXRs from the PIN diode (0.8–4 keV), (d) fast electrons from Cerenkov detectors, (e) the Rogowski dI/dt signal and finally neutrons

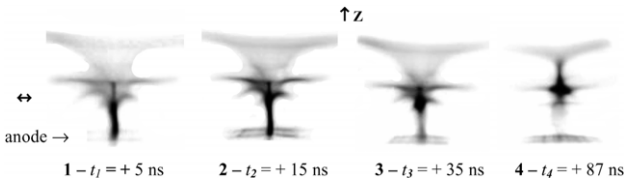

Figure 9. Experimental images of the current cutoff phenomenon (marked by a sign: '↔') taken by the optical image camera with 1 ns time resolution.

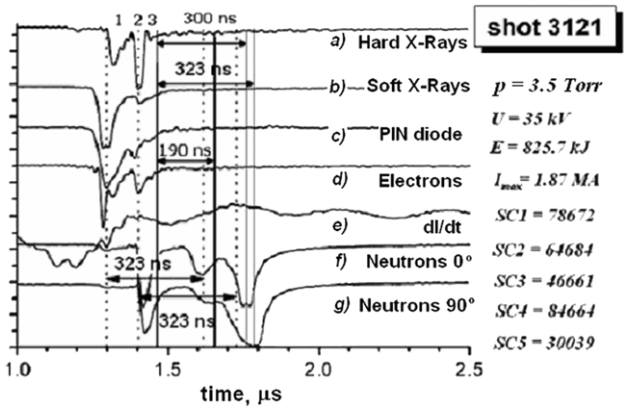

Figure 10. Typical set of registered signals illustrating correlation of various signals versus temporal evolution of neutron emission with its anisotropy data.

plus very HXRs (>80 keV) taken at 90° (f) and 0° (g) by PM tubes + scintillators.

All traces are moved according to the TOF of the corresponding type of radiation, as well as the delay times of related detecting systems (the dead time of PM tubes, cables, oscilloscopes, etc) except neutron pulses which move with their HXR pulses *synchronously* (i.e. by the TOF of HXR).

From these traces, in correlation with figures 6 and 9, one can observe the following features.

(a) SXR pulses from PMT practically coincide with the same from PIN diodes ((*b*), (*c*)) and with maximal plasma compression.

(b) HXRs (a) in the range 8–30 keV (presumably produced by runaways) correctly reflect fast electron signals (d) taken by Cerenkov detectors (pulses 1, 2 and 3) with one exception: the first and most intense pulse from Cerenkov detectors does not correlate with the above HXR trace; probably it is related to HXR of higher energy than the range 8–30 keV, because it is correlated with the beginning of the very HXRs seen on the two bottom traces.

(c) The 1st maximum of the neutron signal $Y(t)$ ((f), (g)) appears 323 ns after the SXR pulse maximum (PIN, PMT); this time interval is exactly equal to the TOF of 2.45 MeV neutrons from the pinch to the PMT; these maxima of both first neutron pulses delayed by 323 ns practically coincide with their first HXR maxima, and it is so for both (0° and 90°) directions again as for the shot reflected in figure 8; synchronization with figure 6 shows that the 1st neutron pulse coincides with maximal plasma compression and heating of at least its electron component.

(d) The second maxima of the neutron signals registered in both directions correlates with the second, relatively small, SXR pulse as well as with the HXR signals and the electron beam pulse. Again, as in the case of figure 8, the *side-on* N pulse is late for the start of its HXR pulse by 323 ns. However, the *head-on* N pulse is delayed only by 300 ns in relation to the moment when the *side-on* pulse appears inside the chamber; this means that the head-on neutrons have higher energy. Thus, if one moves this head-on pulse to its real place on the trace (the start should coincide with the start of the N pulse seen at 0°) it should be delayed by 23 ns in comparison with the side-on N pulse. After this procedure one can see that *both* second N pulses registered in two directions (0° and 90°) start with the beginning of HXR pulses, as in figure 8. Again, as in figure 8, both second pulses reach their maxima at the decay of their HXR pulses.

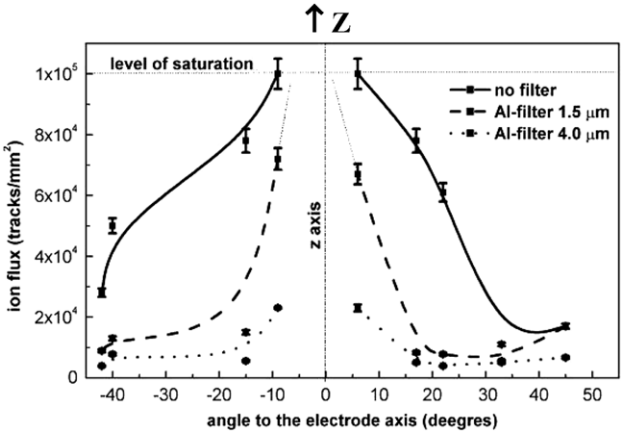

Figure 11. Angular distributions of fast deuterons deduced from track detector samples subjected to direct ion irradiation.

(10) The samples of nuclear track detectors were irradiated by fast deuterons emitted from a single PF-1000 shot, the same as in figure 10. After the irradiation these samples were etched under standard conditions and scanned with an optical microscope. The optical analysis shows the ion crater densities ranging from 10^3 to 10^5 craters mm^{-2} with this number increasing to the Z-axis up to a saturation level. To understand the results obtained we have to take into account the energy losses of D^+ ions in Al foils (D^+ ions of energy >250 keV can penetrate through about a 1.5 μm Al-foil and 500 keV ions through a 4 μm Al-foil) and the detection characteristics of the used detector [11, 12]. Thus, one could estimate that the uncovered detector samples recorded D^+ ions of energy above 80 keV, samples covered with a 1.5 μm Al foil registered D^+ ions more energetic than 330 keV and samples masked with a 4 μm Al foil revealed tracks of ions of energy >580 keV. It was, however, observed that this *fast* ion emission is not reproducible from shot to shot (at least less reproducible than the neutron yield), but its absolute yield as usual decreases with an increase in the filling pressure. Angular distributions of primary deuterons, having different energies and obtained in the above-mentioned shot, are presented in figure 11. In fact, the area of our track detector near the Z-axis was damaged in spite of its distant position from the pinch.

(11) Our miniature ion pinhole cameras show the track distributions as presented in figure 12. It is clearly seen

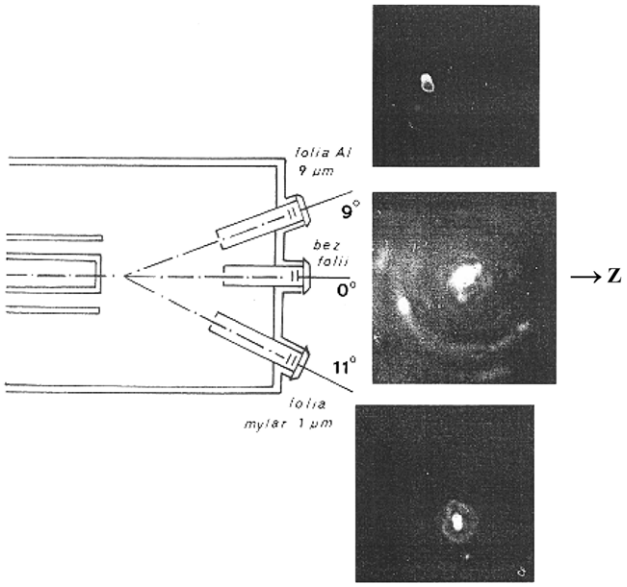

Figure 12. Spatial distribution of tracks received by three ion pinhole cameras placed at different angles to the Z-axis of the chamber.

that the image (an 'autograph' of the fast ion beam) has a tubular structure with an additional very bright maximum on the Z-axis.

(12) In the frame pictures (see figure 13) taken in the visible range with a 1 ns time resolution we found some structure within a zone above the pinch (on the right-hand side of frames (*b*) and (*c*)) which has good correlation with figure 12. This *tubular-conical* formation with a central stem (also of conical shape) always appears *after* the pinching period. (The pinching process is always accompanied by a characteristic *hemispherical* shock wave—see figure 13(*a*)).

These structures become visible right after the moment of current abruption. They changed from shot to shot by cone angle (e.g. the half-angle in (*b*) is 20° whereas in (*c*) it is about 35°) and by their transverse 'layers' (bright discs). For example, in both figures the thicknesses of these discs are less than 3 mm. But in (*b*) one may see just two of them separated at a distance of 10 mm whereas in (*c*) there are three discs with distances between them of 5 and 8 mm from left to right, respectively.

5. Discussion

In paper I we presented results on the main parameters of pinch plasma measurements as well as on their evolution during the period of generation of hard radiation. If the GPM [7] is valid this pinch is presumably a target, which would be irradiated by a fast ion beam generated within a DPF after current abruption phenomenon. The Bennett equation being possibly correct during the period of plasma confinement time (the so-called 'first compression') can help in the estimation of plasma density during the first neutron pulse (see paper I [6]): $0.8 \times 10^{19}\,\mathrm{cm}^{-3}$. The pinch radius also determines the *maximum* value of the azimuth magnetic field at the pinch's border:

$$B_{\max} = 0.2I/r^2 = 2\,\mathrm{MG}, \qquad (3)$$

where $I = 2\,\mathrm{MA}$ and $r = 0.45\,\mathrm{cm}$. This means that the Larmor radii of fast (100 keV) electrons and deuterons, widely presented in the discharge, are accordingly [13]

$$r_{\mathrm{Be}} \geqslant 3.37(W_\perp)^{1/2}/B_\varphi \quad \text{and} \quad r_{\mathrm{Bd}} \geqslant 204(W_\perp)^{1/2}/B_\varphi, \qquad (4)$$

where transverse energy $W_\perp$ is in eV, B_φ is in Gauss and r is in cm. It gives estimations for the *minimal* values of $r_{\mathrm{Be}} \geqslant 5\times10^{-4}\,\mathrm{cm}$ and $r_{\mathrm{Bd}} \geqslant 3\times10^{-2}\,\mathrm{cm}$. They both appear to be much less than the pinch diameter. As for the compressed B_z component being of the order of $10^5\,\mathrm{G}$ (see paper I [6]), these values are, respectively, 100 μm and 0.6 cm.

As was found in paper I the pinch's column during the first neutron pulse is straight and has a height of 10 cm with a radius of ∼0.45 cm. Later on this plasma column is widened and disturbed by instabilities. All pinch parameters start to fall with the characteristic time of the order of the above plasma *confinement time* (∼150 ns). As was shown in paper I the coefficient of the pinch longevity is 10–15 times larger in comparison with the ideal MHD confinement time. And as a consequence its *effective* expansion velocity v_{exp} is also 10–15 times lower compared with the implosion one v_{im}, i.e. $v_{\mathrm{exp}} \leqslant 0.5\times10^7\,\mathrm{cm\,s}^{-1}$. It is supported by the frame-by-frame pictures showing that to the moment of the maximum of the second neutron pulse the radius of the pinch is 1 cm.

Strong perturbations of the plasma sheath surface can be found after the confinement period in all its frame images. The pinch usually breaks into two (or sometimes several) cylinder regions along the column. It looks like a fast penetration (emission) of plasma into the surrounding magnetic field at the periphery of the pinch in the form of a meniscus, i.e. a disc centred at a certain point on the pinch axis and slightly concaved up to the cathode. For a pinch column it gives the impression of being like a gap creation, which 'breaks' the column in the transverse direction to its length. Examples are shown both in figures 9 and 13 of this paper and in some figures of paper I, but in particular in figures 7(*d*) and 14 of paper I [6]. It is seen that the plasma does *not* push away (disappear) from this gap, but becomes of a lower density compared with the adjacent parts of the pinch above and below this 'gap'. A typical size of this zone along the Z-axis (the gap's width) *seen in the figures* is about 1 mm, which is much larger than the electron Larmor radius, but is comparable to the ion one for the B_φ field, which is lower than its above-mentioned maximum during the process of its diffusion into the pinch plasma (see equation (4)).

We shall start our discussions concerning fusion events taking place in PF-1000 with estimations of the possibility of a *thermonuclear* mechanism for neutron generation during first and second pulses. We shall assume that the first pulse is produced by a compression of a fast moving ($3.5\times10^7\,\mathrm{cm\,s}^{-1}$) plasma-current sheath (PCS) with the transformation of the energy of its direct movement (quasi-cylinder shock wave) into heat with additional subsequent adiabatic compression (the temperature increase factor is about 1.4 [14]). As for the second neutron pulse we shall propose at first that it is generated by the second subsequent plasma compression.

Taking into consideration plasma parameters during the first period of the plasma confinement (see paper I [6])—its ion density $n_{\mathrm{i}} \cong 0.8\times10^{19}\,\mathrm{cm}^{-3}$, ion temperature $T_{\mathrm{i}} \cong 1.3\,\mathrm{keV}$, pinch dimensions $R_{\mathrm{p}} \cong 0.45\,\mathrm{cm}$ and $h_{\mathrm{p}} \cong 10\,\mathrm{cm}$ and pinch longevity $\tau \cong 1.5\times10^{-7}\,\mathrm{s}$, we have [13]

$$Y = (n_{\mathrm{i}}^2/4)\langle\sigma\upsilon\rangle_{\mathrm{DD}}\pi R_{\mathrm{p}}^2 h_{\mathrm{p}}\tau \cong 1.5\times10^{10}\,\mathrm{n\,pulse}^{-1}. \qquad (5)$$

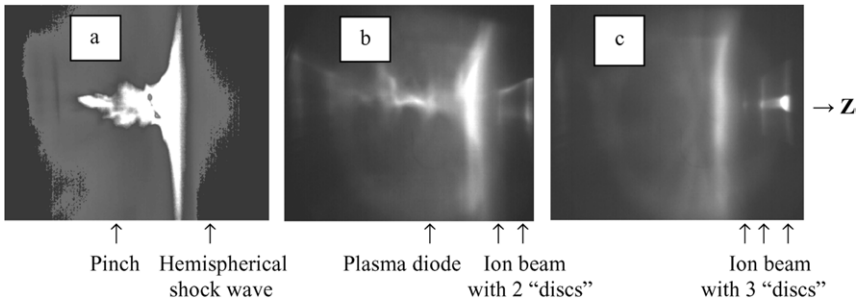

Figure 13. 1 ns pictures taken in the visible range for three different shots and demonstrating a shock wave produced by a cumulative stream during the plasma pinching (*a*) and an ion beam structure as it appears after the current abruption phenomenon (*b*) and (*c*).

This amount is ten times less than the total neutron yield of the device ($(1–2)\times10^{11}$ n pulse^{-1}), and it coincides with the results of measurements made by PM tubes (figures 8 and 10).

As for the more hypothetical 'second compression' (see, e.g., figure 9 the 4th frame taken at the moment $t = +87$ ns, the picture looks as it should for this event, being however 100 ns earlier than one can expect according to the second neutron pulse maximum), we have to nevertheless substitute figures really seen for the moment of the 2nd neutron pulse maximum ($t \cong +180$ ns): for the pinch radius $R_p \cong 1$ cm, ion density $n_i \cong 2 \times 10^{18}$ cm^{-3} (calculated due to pinch radius change) with other parameters having the same values. In this case in order to obtain from formula (5) an experimentally measured real neutron yield 2×10^{11} n pulse^{-1} we have to assume that the ion temperature during this interval of time should be increased to the level of $T_{i\,\mathrm{eff}} \geqslant 4$ keV.

The most dubious data in both cases are the ion temperatures, which were not measured here directly (and have not been reliably measured in all previous experiments). Let us check the possibility of the existence of these temperatures in a real situation. We can estimate the mean-free path of ions in our plasmas by using the following equation [15]:

$$l_{ii} = 3 \times 10^{18} T_i^2 / n_i, \tag{6}$$

where l_{ii} is in cm, T_i in keV and n_i in cm^{-3}. The results are shown in table 1.

It is clearly seen that if for the first compression the mean-free path of ions is smaller compared with the pinch's dimensions, the plasma of the 'second one' should be collisionless.

Estimations of the characteristic *collision rates* can be made using equations [15, 16]

$$\upsilon_e = 2.9 \times 10^{-6} n \lambda T_e^{-3/2}, \tag{7}$$

$$\upsilon_i = 3.4 \times 10^{-8} n \lambda T_i^{-3/2}. \tag{8}$$

These estimations have supported the above conclusion: for the first compression stage equilibrium for electrons and for ions is established for less than 0.2 ns and 20 ns, respectively, which is short compared with the duration of this phase (150 ns). The time to achieve *thermal equilibrium between* ions and electrons (here we have presumably ion heating by SW and adiabatic compression) would be $(m_d/m_e)^{1/2} \cong 60$ times longer. It would mean that even here electrons might not have enough time *to reach the level of ion temperature*. In contrast, the above time intervals for the hypothetical 'second compression' (20 ns and 2 μs for electrons and ions separately and even larger for their mutual equilibrium) are substantially longer than the duration of the second neutron pulse.

One can now see that the first pulse can be explained *in principle* on the basis of shock wave/adiabatic plasma compression and heating. Conversely, for an explanation of the generation mechanism of the second neutron pulse we have to come up with other ideas.

According to our analysis of the data obtained here we have evidence of the virtual plasma diode creation at the PF-1000 facility. That is we have here the same phenomena which were investigated in the FLORA device [3, 4, 14] and proved in those experiments by almost the same set of diagnostics as here but additionally supported there by 1 ns multi-frame laser interferometry.

Indeed till the moment of the current maximum the main part of electric energy accumulated previously in the bank is concentrated as magnetic energy near the pinch column, i.e. in the 'plasma inductive storage'. Then we have an abruption in the current and the formation of a plasma diode on the pinch. The effects in the diode lead to an evolution following the scenario (compare the experimental sequence of frames in figure 9 presented in the lower part of the double-pinch structure—see paper I [6]—with the schematic drawing of figure 14(*a*) made for this lower pinch and with figure 14(*b*), where the region of the EMH effects [8] is shown on an enlarged scale).

(1) *Rayleigh–Taylor instability* development on the surface of the pinch (with an increment in the unstable state development of the order of 10^8 s^{-1}).
(2) Formation in a certain pinch region along the perimeter of the pinch column (*above* plasma neck but *below* plasma widening—i.e. in a region shown by the symbol '↔') of the *right-hand-triple* of vectors $\{\boldsymbol{H}_\varphi, \mathrm{grad}\, n, \boldsymbol{V}_h\}$, where the vector $\boldsymbol{H}_\varphi$ is the azimuth magnetic field of current, grad n is the plasma density gradient and $\boldsymbol{V}_h$ is the vector of the magnetic field penetration direction.
(3) Fast increase in the *anomalous resistivity* R_{an} in this ring-like region of a skin-layer because of a number of microinstabilities (with increments of the order of 10^{13-11} s^{-1}) provoked by the EMH field effects, which resulted in *plasma disc-like release* outwards from the pinch (practically with gas-dynamic velocity of the penetration into the 'confining' magnetic field $\boldsymbol{H}_\varphi$) as well as in the fast *meniscus-like convective penetration of the magnetic field* into plasma (anomalous resistivity R_{an} can be deduced from the electro-technical measurements of current and voltage across the pinch column and also evaluated from EMH theory [8]).

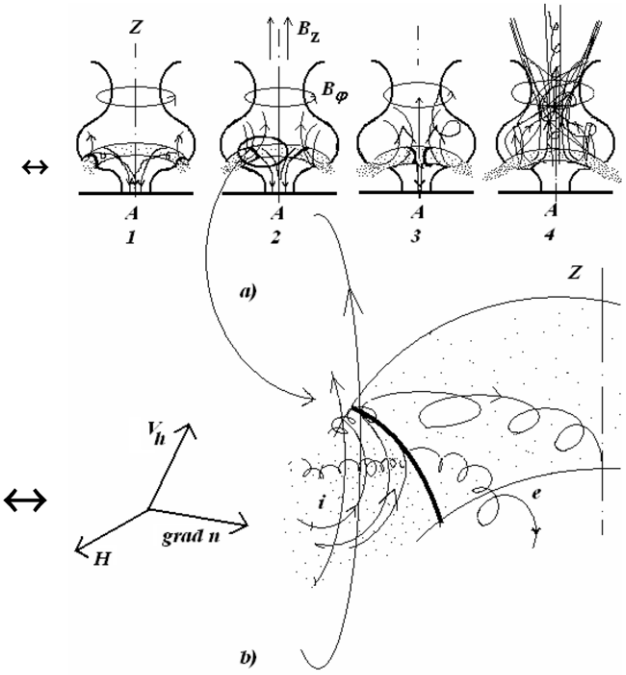

Figure 14. Model pictures of the plasma diode evolution (*a*) and (*b*) based on [3, 8, 14].

(4) *Current cutoff* within the skin-layer due to R_{an} followed by induction of a high vortex *electric field* $\boldsymbol{E}_{ind}$ according to Maxwell's equation: $\partial \boldsymbol{H}/\partial \sim \mathrm{rot}\, \boldsymbol{E}_{ind}$ inside the gap of the magnetic field penetration; thus, this process forms a virtual 'plasma diode' with the 'anode' width of the order of the pinch diameter and the 'anode–cathode' separation determined by a subsequent process of e-beam formation based on a parapotential model [16, 17], which permits the carrying, through the gap, of the e-beam I_b of about the same current magnitude as the previous collisional current I_c:

$$I_b \cong 8500\beta\gamma r/d[\mathrm{A}] \approx I_c, \tag{9}$$

where β and γ are relativistic factors, r/d is the so-called *aspect* ratio, i.e. the ratio of the radius of the diode $r \approx r_p$ to the distance d between the virtual anode and the cathode, and I_b and I_c are in amperes.

(5) *Acceleration of electrons* by the above field ($\boldsymbol{E}_{ind} \sim (\Delta \boldsymbol{H}/\Delta t) \times d$), generated during the cutoff process, where $\Delta \boldsymbol{H} \sim 0.2 I_p/r_p$, Δt is the current's cutoff time ruled by increments of microinstabilities and measured by the rise-time of the second HXR pulse and d is the diode separation, defined from equation (5) and estimated from figure 9 or from figures 7(*d*) and 14(*a*) of paper I.

(6) *Self-focussing of the e-beam* inside the pinch and the *propagating* of it right up to the anode (see, in figure 9, images related to the moments $t_1 = +5$ ns and $t_2 = +15$ ns and the schematic drawing in figure 14(*a*) in the sequence 1, 2, 3).

(7) *Interaction of fast electrons* with the anode surface, resulted in production of *HXRs* and *vapours* of anode material glowing in the visible and the SXR range (figure 9, frames 2 and 3).

Table 1. Estimates of the mean-free paths of ion–ion collisions in *thermal* plasma for the first and second neutron pulses for different diameters and heights of the pinch.

Neutron pulse	Time of pulse maximum (ns)	$T_{i\,eff}$ (keV)	n_i (cm^{-3})	R_p (cm)	h_p (cm)	l_{ii} (cm)
First	0	1.3	8×10^{18}	0.45	10	0.6
Second	+180	4	2×10^{18}	1	10	24

(8) *Magnetization of the fast electrons* after penetration of the magnetic field up to the centre of the virtual diode; this comes from the fact that the Larmor radius of electrons is short compared with the diode gap d—see the disappearance of the *filament* luminescence between the diode and the anode in figure 9 ($t_3 = +35$ ns and $t_4 = +87$ ns) and the corresponding explanation in figures 14(*a*) and (*b*).

(9) *Substitution of the e-beam* by the *i-beam*, taking place *simultaneously* with the above process; it becomes possible because the Larmor radius of the accelerated ions is larger than d; the currents of the fast electron and ion beams carry approximately the total pinch current I_p during the time interval τ, for the period of which the plasma inductive storage releases its magnetic energy into anomalous resistivity of the virtual diode:

$$\tau = L_{int}/R_{an}, \tag{10}$$

where L_{int} is the internal inductance of the discharge chamber (probably with some part of the external one related to the part of the electrical circuit adjoining the DPF chamber).

Later on, these parts of the fast ions, which were accelerated to *medium* energy (i.e. to the energy at which their Larmor radius in the magnetic field inside the pinch is of the order, or less than, the pinch radius), should be magnetized. It takes place mainly above the virtual diode gap, i.e. inside the upper part of the pinch [3, 4]. They gyrate during the time interval determined by their confinement time, which could be, in principle, longer than that given by (10) and even longer than the plasma diode existence time. During this *confinement time of fast ions* they interact with the pinch plasma ('hot target') [3–5].

To 'fill' the whole pinch volume by these medium-energy ions, to confine them there and to give them the possibility of going away eventually from the pinch we have to suppose the existence of a longitudinal component of magnetic field (along the Z-axis) $\boldsymbol{H}_z$. Its origin, magnitude ($|\boldsymbol{H}_z| \sim 0.1|\boldsymbol{H}_\varphi|$) and stabilizing effect on the pinch were discussed in paper I [6] (see also the corresponding references there).

Now let us see how this overall physical picture is reflected in our full-scale experiment at the PF-1000 facility fulfilled with a number of different diagnostics and what are the magnitudes of the parameters appearing in the above-mentioned model. In these discussions we shall widely use the results of paper I giving us the temporal behaviour of dense plasma ('pinch', 'target') parameters.

Let us examine the possibility of applying to our case the above-mentioned model based on the virtual plasma diode, the direct production of neutrons by fast ions and ion beam heating of the pinch plasma. We first check the validity of the parameters measured here with the model's variables.

1. *Diode geometry*

To be in conformity with formula (9), assuming the current of fast electrons (for $E_e \cong 100$ keV, $\beta = 0.62$, $\gamma = 1.28$) of the order of the pinch current, we shall have for our virtual diode ($r \cong 0.45$ cm) $d \cong 0.15$ mm, i.e. for 100 keV particles we have to have a vortex field $\boldsymbol{E} \cong 10^7\,\mathrm{V\,cm^{-1}}$; at the same time by these estimations the validity of the demands on the magnetization of the electrons and the free-streaming of the ions within this diode is established (see equations (4)):

$$r_{Be}(\geqslant 5\times 10^{-3}\,\mathrm{cm}) < d < r_{Bd}(3\times 10^{-2}\mathrm{cm}). \qquad (11)$$

2. *Current abruption time*

Estimations using the Maxwell equation: $\boldsymbol{E} \cong \boldsymbol{\Delta H} \times \boldsymbol{\Delta} x/\boldsymbol{\Delta} t$ (where dimensions are in $\mathrm{V\,cm^{-1}}$, G, cm and s, respectively), gave us for the above $E \cong 10^7\,\mathrm{V\,cm^{-1}}$ $\boldsymbol{\Delta} t \cong 10^{-11}$ s, which is short compared with the resolution time of our PMT channels (pulse rise-time) for the HXR pulse (the fact supported by experiments) and is of the order of the ion-sound instability increment.

3. *Beam existence time*

Now we can estimate the diode impedance: $R \cong U/I \cong 10^5/2\times 10^6 = 5\times 10^{-2}\,\Omega$ ($U \sim E \times d$). This is a rather poor value—in the best devices the impedance can be up to 0.3–0.5 Ω [1, 2]. According to equation (10) with the inductance of our 'plasma magnetic storage' equal to $\sim 10^{-8}$ H we shall have for the energy release time τ_L from the plasma inductive storage

$$\tau_L \cong L_{int}/R = 200\,\mathrm{ns}. \qquad (12)$$

The real time of the ion beam existence should be at least 2 times shorter (ions substituting electrons), i.e. $\tau_i = 100$ ns. In fact, as is seen from the oscilloscope traces of figure 10, the HXR pulse at its FWHM is 50 ns. The same should be right for the ion beam. Thus let us count $\tau_i = 50$ ns. It is noticeably shorter than the neutron emission duration in the normal regime and in particular for the case of the 'cusp-like' plasma configuration (see paper I [6]). Together with the fact of the vanishing plasma diode after the moment of about +250 ns in the pictures it means that *the confinement time of fast ions* within the plasma cloud is large compared with the diode existence time and in particular with the time of the energy release from plasma inductive storage.

4. *Energy of the beam*

Now we can estimate the overall energy of the e- and i-beams:

$$W = I \times U \times \tau \cong 2\times 10^6 \times 10^5 \times 10^{-7} = 20\,\mathrm{kJ}. \qquad (13)$$

It gives the efficiency of the beam generation on the level of about 2.5% from the power circuit consumption. Taking into consideration the figures for the highest beam efficiency reported by the Kurchatov Institute team (20%), the Limeil Laboratory (20%), and the Lebedev Institute team (10%), measured by different methods, the figure obtained must be considered to be a very modest one.

Let us examine the possibility of the above *containment* of the fast ion beam inside the pinch. As was shown the *minimal* ion *Larmor radius* in the azimuth field is much smaller than the size of the pinch. We can now estimate the *minimal* average *magnetic field* magnitude (for both H_φ and H_z) inside the pinch provided that the ion Larmor radius is about the pinch radius:

$$B \geqslant 204(W_\perp)^{1/2}/r_{Bd} \cong 3\times 10^4\,\mathrm{G}. \qquad (14)$$

It is close to the above estimate. To have a rough figure for the coefficient of the fast ion 'magnetization' we must compare their direct-flight time through the pinch's length l_p with the duration of the second neutron pulse τ_n. We shall have for the group of ions having energy $E_i = 100$ keV

$$k = \tau_n/(l_p/v_i) = 1.5\times 10^{-7}[\mathrm{s}]/\{10[\mathrm{cm}]/3 \times 10^8[\mathrm{cm\,s^{-1}}]\} = 4.5. \qquad (15)$$

Now we can estimate the *concentration* of the 100 keV ions *inside the pinch* during their confinement period provided that the pinch radius is 1 cm, its height is 10 cm and that all other parameters are the same. Then the length of the fast ion bunch in a free space should be $l_b = v_i \times \tau_i = 15$ cm, the cross-section of the bunch inside the pinch is 3.14 $\mathrm{cm^2}$, the effective volume of the bunch (provided that it is not widened, which is true inside the pinch) $V_b = l_b \times S_b \cong 50\,\mathrm{cm^3}$, the full energy in the bunch $E_b = 10^4 J = 6\times 10^{22}$ eV, the total number of ions in the bunch $N_{tot} = E_b/E_i = 6\times 10^{17}$ particles, the concentration in the bunch $N_{i0} = N_{tot}/V_b \cong 10^{16}\,\mathrm{cm^{-3}}$ and taking into consideration the above coefficient of magnetization we shall have the fast ion concentration inside the pinch:

$$N_i = N_{i0} \times k \cong 5\times 10^{16}\mathrm{cm^{-3}}. \qquad (16)$$

According to the track detector measurements (see above) the main part of our fast ions *abandoning* the pinch is concentrated approximately within the energy range below 200 keV. Unfortunately, it is difficult to say how representative this measured part of fast ions is. Namely, the surface covered by fast ions at a distance of about 0.5 m and giving a possibility of investigating these fast ions (*if* the ion beam preserves its contents within the cone of about 20°–30° with a stem of just a few degrees at this distance) should be, in our case, of the order of 0.1 $\mathrm{m^2}$. That is, this area could collect, in the unsaturated regime, only the number of ions N, which escaped the pinch:

$$N \sim 10^5[\mathrm{d\,mm^{-2}}] \times 10^5[\mathrm{mm^2}] \cong 10^{10}\ \text{ions}.$$

This is about 10^{-8} from the overall number of generated fast ions. Moreover, it seems that our high-current ion beam can exist as a beam only from the rear side (behind) of the SW front, where it can be compensated by an electron back-current inside the cloud of a compressed ionized plasma. After penetrating the SW front (which is about 30 cm from the anode till this moment) and injecting into a neutral gas of low density, where the mfp of fast ions is long compared with the geometry of the main part of it, the ion beam has to be disintegrated. But even the remaining part of the ion beam will still be of much higher concentration compared with the saturation level of the track detectors. Thus, all *measured* ions are distributed at a distance of 0.55 m from the anode on the periphery of the near-axis zone in an arbitrary manner. However, in spite of the facts described here it is reasonable to suppose that the energy range of our 'acting' fast ions (i.e. those mainly *captured* inside the pinch and producing neutrons— not those, which *escaped* the pinch) falls within the energy spectrum interval of about 10–100 keV.

Neutron spectra, depending on the energy of the fast deuterons E_d bombarding the deuterium gas/plasma target and the angle of their registration Θ, will have a peak at an energy E_n, which can be deduced from the equation [18]

$$E_n = (3.269[\mathrm{MeV}]) + E_d + 2\sqrt{2}(E_n \cdot E_d)^{1/2}\cos\Theta. \qquad (17)$$

For $E_d = 0$ and $\Theta = 90^\circ$ we shall have, as well known, $E_n = 2.45$ MeV. At the same time for *our* data on a side-on spectrum of DPF, which demonstrates the same peak position, it only means that the energy (and velocity) distribution of fast ions is peaked at 0 MeV, i.e. we might have rotations of fast ions in both directions *around* the Z-axis—clock-wise and counter-clock-wise—equally possible. It is so, in particular, because estimations of the probable plasma temperature deduced from the FWHM ΔE of the spectra in this very direction ($\Delta E = 72.5(T_{pl})^{1/2}$) usually gave us a value of about 3–4 keV, which is impossible as we have shown above. However, it should be noted that neutron spectral measurements have not been provided in these series of experiments.

The head-on neutron spectra for the energy of fast ions of $E_d = 100$ keV moving *along* the Z-axis and *producing* these neutrons gave us the following data for its peak: $E_n = 2.85$ MeV. This is reflected in the anisotropy factor, which is connected with the energy of fast ions (neutron energy spectrum shift) according to the kinematics of the reciprocal fusion reaction [18].

The neutron yield distribution in different directions to the path of the beam of fast deuterons in the case of 100 keV deuterons will look as shown in figure 15. The angular distribution of the cross-section in the centre of the inertia system is described by the formula

$$\sigma(\Theta) = \sigma(\pi/2)(1 + A\cos^2\Theta). \qquad (18)$$

We compared the data for the experimental coefficient A measured by many authors in the 1950s and 1960s for different energy ranges of deuterons and in various geometries of experiments and took its value for our case to be equal to 0.8.

A comparison of the experimental data of figure 7 with the computed ones according to equation (17) demonstrates fairly good agreement. One has to take into account that because our chamber is made of steel with thick walls we put our activation counters at positions where the thickness is the same for all directions except 180°. But our estimations have shown that the influence of the materials in this direction (copper anode lid and stainless steel flange) on neutron penetration is about the same as in all other directions. However, the experimental curve has two distinctions: the absence of the yield's decrease ('neck', 'waist') on distribution at 90° and slightly lower values of the yield along the Z-axis (0° and 180°). However, if one takes into account rotations of the entrapped fast ions inside the pinch in contrast to the parallel beam, they both vanish, first by the disappearance of the distribution valley and subsequently the ratio of the yields.

We can now estimate two things—direct neutron production by *fusion collisions* of these *magnetized* ions with plasma and plasma *heating* because of *Coulomb interaction* of these fast magnetized ions with the pinch's plasma.

Let us examine first a relaxation of the ion beam inside the pinch. We shall be interested whether our ion beam can lose its energy and add it to the bulk plasma by a comparable degree in relation to the pinch's own energy content.

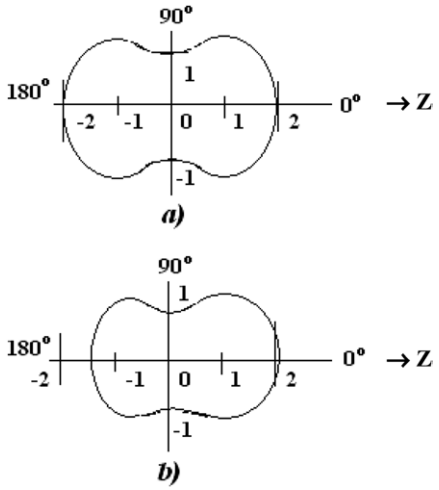

Figure 15. Theoretical angular distribution of neutron intensity produced in a thin gas target by a low-intensity parallel beam of 100 keV deuterium ions as test particles: (*a*) in a centre-of-mass system and (*b*) in a laboratory coordinate frame.

It is a well-known fact [15, 16, 19] that fast ions of energy E_i lose their energy to the bulk plasma via Coulomb collisions with *field* electrons and/or ions depending on the plasma temperature T_{pl}. When $E_i > (m_i/m_e)T_i$ the ions are cooled by Coulomb drag on electrons and undergo little angular scattering. Within the range $T_i < E_i < (m_i/m_e)T_i$ most collisions happen with *field ions* and a strong *scattering* of ions occurs. In our case the above latter energy interval lies in the range between 10 and 400 keV.

We shall use for these estimations the following equation valid for the so-called 'slowing-down' time $\tau_s^{i/i}$ of the deuterium i-beam relaxation on *field ions* (the energy loss time for this beam is correspondingly longer by a factor of $(m_i/m_e)^{1/2}$) [15, 16]:

$$\tau_s^{i/i} = (2)^{1/2}E_i^{3/2}/9 \times 10^{-8}\ n_i\lambda, \qquad (19)$$

where λ is the Coulomb logarithm, e is the electron charge and E_i is the energy of fast deuterons in eV. This formula is true if $m_i V_i^2/2kT_i \ll 1$ as in our case. Taking into account the pinch's radius, its height (1 cm and 10 cm, respectively) and its ion density 2×10^{18} cm^{-3} one can see that the *'slowing-down' time* of 100 keV ions is 2.4×10^{-8} s (i.e. smaller compared with the neutron pulse duration time). It gives the mean-free path of 7 cm for the slowing-down time (strong scattering of ions on ions), whereas to establish the Maxwell distribution function the time will be about 1.5×10^{-6} s. For ions within the energy interval 10–100 keV it will be noticeably shorter. On the other hand, ions in the above energy range (velocities $(1–3) \times 10^8$ cm s^{-1}) being magnetized should make 2–10 rotations inside the pinch during the neutron pulse duration (150 ns) thus increasing their trajectory length to ~50–200 cm during the *plasma* confinement time.

Now let us check the slowing-down time of these ions on *field electrons* for our case $m_e V_i^2/2kT_e \ll 1$ (where T_e is the field electron temperature):

$$\tau_s^{i/e} = (2)^{1/2}T_e^{3/2}/1.6 \times 10^{-9} n_e\lambda = 5 \times 10^{-8}\ \mathrm{s}. \qquad (20)$$

The result is close to that obtained by equation (19). It is not surprising. The scattering process is greater for particles with smaller velocity differentials. In our case the velocity of fast ions (3×10^8 cm s^{-1}) is about five times higher than the field-ion velocities ($\leqslant 5 \times 10^7$ cm s^{-1}) and also about five times less than the field-electron ones ($\geqslant 1.5 \times 10^9$ cm s^{-1}). However, the ion slowing-down time interval is determined by two–three collisions with ions and about 100 collisions with electrons. This fact explains our estimations made using equations (19) and (20). It means that our fast ions interact with both plasma components in almost a comparable degree with a certain preference for field ions and with one important feature—the scattering character is strong for the ion component changing the direction of the decelerated fast ions, which was mentioned above. Thus, between the two parts of fast ions (approximately quantitatively equal but both small compared with the total number generated in the PF) the group *slowing down on field ions* is *isotropic* in contrast to those stopped by field electrons. Later on, because of the fact that our pinch has a shorter confinement time compared with the ion *energy* loss time (the time of establishment of the new Maxwellian distribution), namely, the first group of decelerated ions will be magnetized and this group will produce the main part of fusion neutrons.

It means that about ~1/8–1/4 of the fast ions will lose their energy inside the plasma. Thus, ≅2 kJ of the beam energy will be deposited inside the pinch within the field particles (mainly on the ion component). As a result, each particle of the ion component of plasma will acquire an additional portion of energy: ~2 kJ $/n_{\mathrm{i}} V_{\mathrm{pl}} \geqslant 0.5$ keV. It is comparable to the initial thermal one (~1.3 keV). At this increased temperature $T_{\mathrm{i}} = 1.8$ keV the mean-free path for ions (equation (6)) is <5 cm—still less compared with the pinch height. It can explain a partial neutron yield increase during the second pulse: according to equation (5) with an increase in volume by four times (radius by two times), a decrease in plasma density by four times, but with an increase in the cross-section of fusion reactions [16] by about ten times:

$$Y = (n_{\mathrm{i}}^2/4)\langle\sigma\upsilon\rangle_{\mathrm{DD}}\pi R_{\mathrm{p}}^2 h_{\mathrm{p}}\tau \cong 4 \times 10^{10}\ \mathrm{n\ pulse}^{-1}. \qquad (21)$$

On the other hand, a 10 kJ beam of 100 keV ions contains 6×10^{17} particles. For these particles equation (5) will look as follows:

$$Y = (n_{\mathrm{ipl}} N_{\mathrm{i\,fast}}/4)\sigma\,\upsilon_{\mathrm{i\,fast}}\pi R_{\mathrm{p}}^2 h_{\mathrm{p}}\tau, \qquad (22)$$

where $n_{\mathrm{ipl}} = 2 \times 10^{18}$ cm^{-3} is the plasma density, $N_{\mathrm{i\,fast}}$ the concentration of fast ions within the pinch and $\upsilon_{\mathrm{i\,fast}}$, σ the velocity of fast ions and fusion cross-section, respectively.

Taking into consideration the concentration of these fast (100 keV) ions in the bunch, their magnetization inside the pinch and using the fusion cross-section for 100 keV deuterium ions equal to 1.5×10^{-26} cm^2 [18] one will obtain a figure for the total neutron yield of 10^{12} neutrons/shot, which is a bit high compared with the best experimental one. But this exaggeration can be easily explained by a lower real concentration of fast ions within the pinch plasma.

The overall result for the fast ion interaction with the hot dense pinch's plasma can be reformulated now in the following manner: the situation for the primary ('thermonuclear') model of neutron production presented in the first hypothesis is remarkably *improved* by the second mode described here. Namely, the above inductive (rapid in comparison with the collisional one!) mechanism of generation of fast ions within the DPF's plasma will form the overall distribution function with an *enriched high-energy tail* that usually produces most fusion reactions.

Now we have to link these results to our data on the ion beam observations made for the *outside* part of the pinch (figures 11, 12 and 13). First let us propose that the conical structures seen in figures 13(*b*) and (*c*) are produced by a beam of fast ions, which escape the pinch and heat/ionize the residual gas/plasma in this zone on the rear side of the SW, thus becoming visible itself. Indeed this explanation of the cone-tubular structure type is quite reasonable. In fact, inside the pinch we have a superposition of longitudinal (captured by PCS and compressed) and azimuth (compressing and diffusing) magnetic fields. And in the centre, as well as outside the pinch (above it), $\boldsymbol{H}_z$ prevails whereas on the periphery *inside* the pinch the situation is in favour of $\boldsymbol{H}_\varphi$. Above the pinch the force lines of the longitudinal (mainly presented here) magnetic field should fan out (diverge in a cone structure).

Because of this, in the close vicinity of the Z-axis fast ions are accelerated along the singularity line of the *azimuth* magnetic field (so without any influence of it) thus forming the above-mentioned stem with a slight divergence. We believe that this stem is reflected in the pictures of figure 13. At the same time the conical-tubular structure of the ions leaving the pinch can be formed by these *higher energy* ions, which made only a few (or just one incomplete) gyrations inside the pinch and were collected near its generatrix. And because the cone-like shape is specific for the upper part of the pinch (and for the longitudinal magnetic field connected with it) their stream acquires this shape. It is seen both in the direct-irradiated track detectors of figure 11 and in the pictures of figure 13.

Because the generatrix of the cone outside the pinch at a distance of about 10 cm has a regular cone shape it is clear that the *external* magnetic field (outside the pinch) cannot change the orbit of 100 keV ions. This means that its magnitude is 10^{-2} MG or less. This is the *upper* limit for $\boldsymbol{H}_{\mathrm{ext}}$ having mainly longitudinal components and produced by the compression of an initial small field as was mentioned above. The *smallest extreme* of the field, at a distance of ~10 cm from the pinch, can be roughly estimated by the inverse quadratic distance law $-\boldsymbol{H}_{\mathrm{ext}} \sim 1/r^2 \sim 10^3$ G.

The situation described above and connected with the disintegration of the ion beam after penetrating the SW front could explain why we cannot see this 'centred ring' in figure 11 but can see it with the ion pinhole chambers in figure 12. Indeed, because this scattering of the ion beam has a random character any pinhole positioned at certain distances from the SW front will form an image of the source of the ions similarly to the optical case of an image produced due to light scattering by an object. At the same time in the above weak fields the Larmor radius of ions of energy above 100 keV will be ~100 cm—i.e. large compared with the value for our distance from the pinch to the SW front and the two copper semi-rings with track detectors. This means that the ions, which travel first along the conical generatrix, later on scatter randomly. This is why we do not see them in figure 11.

But there is something more. The 'discs' (layers) seen in figure 12 and taken with a 1 ns time exposure reflect the temporal structure of the ion beam. Namely, the velocity of

ions is above 3×10^8 cm s^{-1}. In 1 ns they pass a length of less than 3 mm. Namely, this is the width of the discs we saw in the picture (it should be mentioned here that only a small fraction of these fast ions interact with the heat plasma in this rear part of the SW because the collisional cross-section for these ions is low). The verification of the plasma cooling rate (and photo- and triple-particle recombination processes in deuterium gas [20] if it has already become neutral) showed that their time is short compared with 1 ns (our exposure time of the frame camera). It means that the ion beam consists in fact of a sequence of multiple pulses having duration $\leqslant$1 ns each and separated from one another by distances 5–10 mm, i.e. by time intervals 2–3 ns.

In connection with all the above estimations we have to make three remarks. First, examining the virtual diode configuration one can note a very small effective separation between the virtual anode and the cathode—only 150 μm with a large diode aspect ratio. It seems that such a geometry of the diode should be unstable during this unsteady-state plasma phenomenon. Probably it has an oscillating character, which is reflected in those short bunches seen in figure 13.

Second, one can see that estimations made by using equations (5) and (21) are very sensitive to plasma/beam parameters. In particular, this relates to equation (5) where density is presented to the power of 2. Moreover, a thermonuclear reaction rate averaged over the Maxwellian distribution depends on this formula on plasma temperature to the power of 4.5 within the range 1–5 keV (below 1 keV even faster). Thus, in this situation a really astonishing fact is *not* the large neutron yield *variations* in a DPF from shot to shot (usual criticism to this device), but its relatively *stable* average behaviour (within a factor of 2 in good facilities)! Probably this fairly fine performance is an additional argument in favour of the second neutron production mechanism: still fusion head-on impact cross-section on the level of fast ion's energy near 100 keV follows the ion energy change even slower than a linear law. Very likely this remark relates not only to the second neutron pulse but also to the first one: this yield looks more stable than PCS velocity changes. We know that usually when we have fast electrons ('runaways' during the first compression of plasma) we can also expect fast ions.

Our third remark is connected to the ions escaping the pinch in the Z-axis direction. According to our measurements and analysis they have slightly higher energy compared with the 'working ones'. Leaving the pinch they interact inside our large chamber (2 m to the chamber wall) with residual gas having a density of $\sim 2 \times 10^{17}$ cm^{-3} (4 Torr D_2). We suppose here that the effective distance of interaction is equal to $l_{\rm int} = v_{\rm i} \times \tau_{\rm n} = (3\text{–}4) \times 10^8 \times 1.5 \times 10^{-7} \cong 50$ cm. We have also to take into account that the duration of the ion beam (and consequently the volume occupied by it) is three times shorter than the neutron pulse duration (i.e. 50 ns instead of 150 ns) and there is no appreciable magnetization effect. Thus, the ratio of the external neutron yield to the internal one will be

$$N_{\rm n\,(ext)}/N_{\rm n\,(int)} \sim \{(N_{\rm i}n_{\rm i})V\}_{\rm ext}/\{(N_{\rm i}n_{\rm i})V\}_{\rm int} < 1/20. \qquad (23)$$

It means that the neutron yield from the space above the pinch is less compared with the yield from the pinch during the first neutron pulse. For simplicity, here we neglect the ionization loss, which is not low (!); thus the obtained figure has a certain exaggeration. Our preliminary measurements with collimation of the neutron emission from the PF-1000 chamber support the result of equation (23). This is a beneficial consequence of a plasma density increase, its heating and confinement (*hot compressed target*) as well as the *magnetization* of fast ions.

Being guided by these results let us now discuss possible ways for the PF-1000 facility optimization. As was mentioned above, during our experiments we found that a *simultaneous* increase in the charging voltage and the initial gas pressure raises the device neutron yield. We observed that in the ranges of pressure 1.0–3.6 Torr and of voltage 30–36 kV the current of the device increased linearly with both parameters. Thus, in the course we have practically reached the upper limit of the operational regime of our device. At the same time, as seen from the oscilloscope traces in figure 2, the current is not changed during the formidable part of the 1st quarter of the discharge period (after the first 3.5 μs). In fact, it demonstrates that at the end of this time interval the current has the character of a plateau with a tendency for a certain decrease (beginning from the 5th microsecond till the peculiarity occurrs at the 8th microsecond). It means that the internal dynamical inductance of the device (its PCS) increases approximately at the same rate as the quasi-cosinusoid current is increased thus compensating it. So the first step for device optimization could be done by a decrease in the *internal* variable inductance of the DPF chamber executed by anode tube shortening. Indeed because of the coaxial configuration the overall internal inductance of the gun is expressed by the formula

$$L_{\rm int} = 2l_{\sim} \times \ln(R/r_{\sim}), \qquad (24)$$

where $l_{\sim}$ is the length of the part of the anode tube included into the electrical circuit during the PCS travelling *along* it, R is the radius of the cathode rod and $r_{\sim}$ is the radius of the pinch, which is included into the electrical circuit as the variable internal conductor of the coaxial part of the circuit's inductance during the PCS travelling *radially* to its implosion. It is seen that during the run-down phase internal inductance increases linearly with $\boldsymbol{l}_{\sim}$ whereas at the implosion stage its enlargement proceeds much slower following a logarithmic law with radius $\boldsymbol{r}_{\sim}$. Thus, it is seen that this re-design of the anode will give an opportunity for eliminating the 'plateau' on the current waveform and for increasing the amplitude of the discharge current as it is approximated from the current waveform by at least about 30%.

Another opportunity becomes clear from the total *external* inductance measurements. It appears that this is of the order of 20 nH at the present moment. At the same time it is known that an increase in the number of capacitors N in a battery should result in a decrease in its inductance according to a *practical* law valid for large batteries: $L_{\rm ext} \sim N^{1/2}$ (an increase in the battery size and consequently its inductance must be *partially* compensated by the *parallel* operation of the increased number of capacitors). It means that in our case the external inductance for our bank must really be on the level

$$L_{\rm ext} \cong \{(40\,{\rm nH}) : (264)^{1/2})\} \cong 6\,{\rm nH}, \qquad (25)$$

i.e. three times lower in comparison with the actual one. According to our estimations the main impact in our present external inductance is produced by our current collector. Its

new design might improve the situation tremendously. We may expect an increase of the current in this situation by a few times. This hope is based on our previous experience with the PLAMYA facility [1f] where we had a total current of 2.5 MA and a neutron yield (not yet completely optimized due to restrictions implied by the outer diameter of the DPF chamber used) of the level of 2×10^{11} n pulse^{-1} (i.e. practically the same figures as in PF-1000). This was done on the device with an energy storage of only 250 kJ based on the *same type* of capacitors but with a much more compact collector system ($\varnothing \cong 50$ cm) and at the DPF chamber having a relatively shorter anode tube.

One specific detail was very important in our experiments with the PLAMYA device [2]. Namely, inside the chamber we used a disc positioned 10 cm apart from the upper anode plate, which restricted the PCS from moving in an upward direction. The same measurement done recently and investigated in more detail with the support of numerical calculations was performed with an optimization of the PF-3 facility at the Kurchatov Institute [21,22]. In these experiments it was found that the upper disc not only decreases the overall inductance giving rise to a *current maximum by 10%* but what is more important it also moves the current peculiarity (dip) forward in time ensuring an increase in the *pinch* current at the plasma maximal compression under identical conditions *by two times*.

6. Conclusions

According to the results of the entire set of experiments one may see that the main neutron pulse (the second one as usual) is irradiated after the phenomenon of current abruption. This event bears many features inherent to a plasma diode formed in accordance with the electron magneto-hydrodynamic model. The main mechanism of neutron generation is in tune with a GPM whereas three groups of temporal parameters rule the neutron yield.

(1) The time of the energy release from the plasma inductive storage system (magnetic field stored around the pinch) after the moment of current abruption, when this energy is converted into streams of fast electrons and ions, as well as the efficiency of this conversion.
(2) The confinement time of fast deuterons having medium energy (10–100 keV), which are produced at the above current abruption and gyrated in the magnetic field within the pinch.
(3) The confinement time of the pinch plasma (the 'hot plasma target' bombarded by the above stream of medium-energy ions) as well as its density and volume.

The analyses of these results are in favour of the neutron emission model based on ion beam–plasma interaction with three important features: (1) *the plasma target is hot* and confined during more than ten *'inertial confinement times'*; (2) *ions* of the main part of the beam are *magnetized* and *entrapped* about the pinch plasma target for a longer period than the *characteristic time of the plasma inductive storage system*; and (3) *ion–ion collisions* (both *the fusion* ones due to head-on impacts and the *Coulomb* ones due to an increase in the effective temperature of the ion component of the bulk plasma) *responsible for neutron emission*. Fast ions are generated as a sequence of pulses having a duration of less than 1 ns and separated in time by intervals of about 2–3 ns. The part of the ions leaving the pinch in the direction of the Z-axis has a conical-tubular structure. They produce neutrons in a certain volume of residual gas next to the pinch with a total yield much less than that of the main neutron pulses.

An analysis of the results has shown that one of the ways in which a future improvement in the neutron yield of the PF-1000 facility might be achieved by changing the geometry of the device. We believe that the experiments are in favour of the construction of new larger DPF devices, in particular, if based on modern high-current technology. In this case an increase in the plasma volume, the energy of fast ions as well as the longevity of the 'target' and the beams will give additional advantages.

Acknowledgments

The work was supported in part by the International Atomic Energy Agency Grants No 11940, 11941 and 11942 and by the Federal Agency on Atomic Energy of the Russian Federation.

References

[1] Bernard A *et al* 1998 *J. Moscow Phys. Soc.* **8** 1
[2] Mather J 1971 *Methods in Experimental Physics, Plasma Physics* vol 9B ed R H Loveberg and H R Griem (New York: Academic) pp 187–249
Bernard A *et al* 1977 *Nucl. Instrum. Methods* **145** 191–218
Gentiliti A, Maisonnier Ch and Rager J P 1979 *Plasma Phys.* **5** 41
Herold H *et al* 1989 *Nucl. Fusion* **29** 1255–69
Gribkov V A *et al* 1988 Experimental investigations on "PLAMYA" installation *Fiz. Plazmy (Plasma Phys.)* **14** 987 (in Russian)
Freeman B *et al* 2002 *AIP Conf. Proc.* **651** 261–4
[3] Gribkov V A *et al* 1980 *Neutron-Physics Researches (Moscow, Russia), Proc. of the PN Lebedev Physical Institute* vol 127 (New York: Allerton Press) pp 32–61
Gribkov V A and Krokhin O N 1988 The comparative analysis of the DPF devices in the broad energy range *12th Int. Conf. on Plasma Physics and Controlled Nuclear Fusion Research. (Nice)* IAEA-CN-50, C-IV-5-1, p 126 (extended synopses)
Dubrovsky A V 1988 Hard emissions of plasma focus *Candidate of Phys.-Math. Sci. Dissertation* P N Lebedev Physical Institute, Russian Academy of Sciences (in Russian)
Gribkov V A and Krokhin O N 1990 Acceleration processes in a plasma focus *17th IEEE Int. Conf. on Plasma Science, (San Francisco Bay Area)*
Gribkov V A 2000 Pinch methods of plasma generation *Encyclopedia of Low Temperature Plasma* vol 2 ed V E Fortov p 358 (in Russian)
Soto L 2005 *Plasma Phys. Control. Fusion* **47** A361–81
[4] Gribkov V A 1991 Physical processes in high current discharges of the plasma focus type *Doctor of Phys.-Math. Sci. Dissertation* P N Lebedev Physical Institute, Russian Academy of Sciences (in Russian)
[5] Vyskubov V P *et al* 1979 *PN Lebedev Physical Institute Reports* No 12, pp 37–41
[6] Gribkov V A, Bienkowska B, Borowiecki M, Dubrovsky A V, Ivanova-Stanik I, Karpinski L, Miklaszewski R A, Paduch M, Scholz M and Tomaszewski K 2007 Plasma dynamics in PF-1000 device under full-scale energy storage: I. Pinch dynamics, Shock-wave diffraction, and inertial electrode *J. Phys. D: Appl. Phys.* **40** 1977 (paper I)

[7] Krompholz H, Michel L, Schonbach K H and Fischer H 1977 *Appl. Phys.* **13** 29
Schmidt H *et al* 1984 *Atomkernenerg. Kernt.* **44** 191
Jäger U and Herold H 1987 *Nucl. Fusion* **27** 407
Schmidt R and Herold H 1987 *Plasma Phys.* **29** 523
[8] Kingsep A S, Chukbar K V and Yan'kov V V 1987 Electron magnetic hydrodynamics *Voprosy Teorii Plazmy (Problems of Plasma Theory)* vol 16, ed B B Kadomtsev (Moscow: Energoatomizdat) p 209 (in Russian)
[9] Scholz M, Miklaszewski R, Gribkov V A and Mezzetti F 2000 PF-1000 *Nucleonika* **45** 23
[10] Herold H, Jerzykiewicz A, Sadowski M and Schmidt H 1989 *Nucl. Fusion* **29** 1255
[11] Sadowski M *et al* 1994 *Nucl. Instrum. Methods.* B **86** 311
[12] Szydlowski A *et al* 1999 *Nucl. Instrum. Methods.* B **149** 113
[13] Luk'yanov S Yu and Koval'skij N G 1997 *Hot Plasma and Controlled Nuclear Fusion* (Moscow: Moscow Engineering Physics Institute) p 63
[14] Filippov N V *et al* 1971 Experimental and theoretical investigation of the pinch discharge of the plasma focus type *4th Int. Conf. on Plasma Physics. and Controlled. Nuclear Fusion Research (Madison)* (Vienna: IAEA) IAEA-CN 28/D-6
[15] Trubnikov B A 1965 *Reviews of Plasma Physics* vol 1 (New York: Consultants Bureau)
[16] Huba J D 2004 *NRL Plasma Formulary* The Office of Naval Research
[17] Babykin M V 1981 Electron thermonuclear synthesis *Itogi Nauki i Tekhniki (Results of Science and Technology)* ed V D Shafranov vol 2 (Moscow: VINITI) pp 5–79 part 2
[18] Curtiss L E 1959 *Introduction to Neutron Physics* (Princeton, NJ: Van Nostrand)
Grigoriev I S and Meilokhov E Z (ed) 1991 *Fizicheskie Velichiny (Physical Quantities) Reference Book* (Moscow: Energoatomizdat) (in Russian)
[19] Shkarofsky I P, Johnston T W and Bachynski M P 1966 *The Particle Kinetics of Plasmas* (Reading, MA: Addison-Wesley)
[20] Smirnov B M 1972 *Fizika Slaboionizovannogo Gaza (Physics of Low-Ionized Gas)* (Moscow: Nauka) (in Russian)
[21] Karakin M A *et al* 2004 Studies on the liner compression in the PF-3 facility modernized discharge system *15th Int. Conf. on High-Power Particle Beams* (*Beams'04 Saint-Petersburg, 2004*) p 239 Abstracts
[22] Karakin M A *et al* Progress in Filippov-type plasma-focus studies at Kurchatov Institute *Int. Conf. PLASMA-2003 Research and Applications of Plasma (Warsaw, Poland, 9–12 September)* pp I3-3